

# Effect of sintering conditions on microstructure and dielectric properties of $\text{CaCu}_3\text{Ti}_4\text{O}_{12}$ (CCTO) ceramics

Romy Löhnert<sup>1</sup>, Rainer Schmidt<sup>2</sup>, Jörg Töpfer<sup>1,\*</sup>

<sup>1</sup>Department of SciTec, University of Applied Sciences Jena, Carl-Zeiss Promenade 2, 07745 Jena, Germany

<sup>2</sup>Departamento de Física Aplicada III, GPMC, Facultad de Ciencias Físicas, Universidad Complutense de Madrid, 28040 Madrid, Spain

Received: 1 April 2014 / Accepted: 7 January 2015 / Published online: 25 January 2015

**Abstract** The influence of sintering temperature and dwell time on the microstructure formation and dielectric properties of  $\text{CaCu}_3\text{Ti}_4\text{O}_{12}$  ceramics was investigated. For sintering temperatures of 1050 and 1100 °C significant differences in the  $\text{CaCu}_3\text{Ti}_4\text{O}_{12}$  ceramic microstructure and the segregation of a  $\text{CuO}_x$ -rich phase towards the grain boundary (GB) areas were observed with increasing dwell time. In addition to the formation of a semiconducting bulk and insulating grain boundary phase the segregated  $\text{CuO}_x$  forms an intergranular phase, and the effects of this phase on the dielectric properties are rather intriguing. At sintering temperature below 1050 °C only small amounts of  $\text{CuO}_x$  segregate, whereas sintering above 1050 °C (e.g., 1100 °C) leads to increased evaporation of the  $\text{CuO}_x$ . Therefore, the effects of the  $\text{CuO}_x$ -rich intergranular phase upon the dielectric properties are felt strongest in samples sintered at 1050 °C. Such effects are discussed in terms of microstructural variations due to liquid phase sintering behavior facilitated by the  $\text{TiO}_2$ - $\text{CuO}_x$ -eutectic, which appears to be melted at high sintering temperature prior to evaporation of  $\text{CuO}_x$  at prolonged dwell times at the highest sintering temperatures (1100 °C).

**Keywords:**  $\text{CaCu}_3\text{Ti}_4\text{O}_{12}$  · Sintering temperature · Dwell time · Microstructure · Impedance spectroscopy

## 1. Introduction

$\text{CaCu}_3\text{Ti}_4\text{O}_{12}$  (CCTO) has a cubic 1:3 A-site ordered perovskite-related structure with space group Im-3. Cu ions are situated in a square-planar coordination on A' positions of the general formula  $\text{AA}'_3\text{B}_4\text{O}_{12}$  which causes  $\text{TiO}_6$  octahedra to be strongly tilted [1]. Large values of the effective dielectric permittivity of up to  $\epsilon' \approx 10^5$  were reported for polycrystalline CCTO ceramics [2, 3]. Other compounds of the same structural family with A=Pr, Sr, La, Bi and other elements also show high effective permittivity (e.g.,  $\epsilon' \approx 2000$  for  $\text{Pr}_{2/3}\text{Cu}_3\text{Ti}_4\text{O}_{12}$ ) [1, 4, 5].

The high effective permittivity is ascribed to the formation of an internal barrier layer capacitor (IBLC) structure, where grain boundary (GB) regions show larger resistivity than the grain interior bulk regions. Grain boundaries act as internal charge transport barriers along the electrical current percolation path and induce the high overall capacity, i.e., the GB areas resemble a thin layer of dielectric which, at certain frequencies, dominates the dielectric response of the whole sample. The effective relative permittivity  $\epsilon_{\text{eff}}$  that is derived from the capacity of the sample (the symbol  $\epsilon'$  is used from now on) reflects the amplification of the GB permittivity  $\epsilon_{\text{gb}}$  due to the reduced thickness of the GB region  $t_{\text{gb}}$  as compared to the full grain size  $t_{\text{g}}$  [6]:

$$\epsilon'_{\text{eff}} = \epsilon_{\text{gb}} \frac{t_{\text{g}}}{t_{\text{gb}}}$$

The interpretation of this extrinsic effect is supported by previous impedance spectroscopy (IS) measurements, which gave evidence of two different types of electrical conduction mechanisms in CCTO ceramics; semi-conducting bulk and insulating GB regions. At low frequencies the GBs impede current flow and enable a large effective permittivity. At

Corresponding author: J. Töpfer (\*)  
e-mail: joerg.toepfer@fh-jena.de

sufficiently high frequency charge carriers mainly oscillate within the grains and a sharp drop in permittivity to a bulk relative permittivity of  $\epsilon' < 100$  occurs [2, 3, 7, 8]. The macroscopic behavior can be modeled by a series circuit of two parallel RC-elements (R=resistor, C=capacitor) characterizing the bulk and the GB behavior, respectively. IS allows quantitative evaluation of bulk and GB electrical resistivity and permittivity based on complex impedance plots ( $-Z''$  vs.  $Z'$ ), frequency (f) dependent plots of the relative permittivity ( $\epsilon'$  vs. f) and the model series circuit [9, 10].

The origin of the difference in electrical conductivity between GB and bulk regions is not fully understood yet. The difference in activation energy for bulk and GB charge transport is large (up to a factor of 7.5) [7], which clearly indicates different charge transport mechanisms [11]. This could be due to differences in chemical composition between the bulk and GB regions. A  $\text{CuO}_x$ -rich phase segregates at the GBs at high sintering temperatures, however precise experimental evidence of heterogeneous chemical composition is scarce. Recently,  $\text{CuO}_x$  segregation at the sample surface and slight Cu-deficiency in the grain interior on the A' lattice site was demonstrated by quantitative EDX analysis for samples sintered above 1025 °C [11], in agreement with other work [12–14].

The electrical properties of CCTO strongly depend on material preparation and microstructure formation. This is illustrated by the wide span of reported effective permittivity values of CCTO ceramics even if prepared by the same mixed oxide route and conventional sintering. Much experimental work has been devoted to understand the effect of sintering temperature on microstructure formation and electric properties [11, 15]. Less attention has been paid to the effect of dwell time. At a sintering temperature of 1100 °C, an increase of the effective permittivity was reported with prolonged dwell times, whereas grain growth was limited [16–18]. It was shown that the amount of  $\text{CuO}_x$ -rich GB phase was reduced at longer sintering times [16].

In this study the effects of both, dwell time and sintering temperature on microstructure formation and electrical properties of CCTO ceramics are investigated in detail. Since both, bulk and GB resistivity are expected to be sensitive to sintering conditions [11], impedance spectroscopy was used to analyze the electric properties of samples sintered with different dwell times and sintering temperatures. As result, a detailed picture of the formation of a heterogeneous microstructure in CCTO ceramics including the formation of an intergranular phase besides the insulating grain boundary phase is presented here, and correlations with electric properties are discussed. From the results a model of the formation of IBLC structure in CCTO is derived.

## 2. Experimental

CCTO ceramics were prepared by the mixed oxide route. Stoichiometric amounts of  $\text{CaCO}_3$  (98.0 %, Merck),  $\text{CuO}$  (99.7 %, Alfa Aesar) and  $\text{TiO}_2$  (99.5 %, rutile, Tronox) were homogenized in deionized water. During calcination at 970 °C for 6 h the CCTO phase was formed. The powder was wet milled to a particle size of 1.0  $\mu\text{m}$  in a planetary ball mill (Pulverisette 5, Fritsch) using zirconia vessel and media. Pellets of 15 mm diameter and 2 mm thickness were prepared by uniaxial pressing. The samples were sintered at temperatures of 900, 950 and 1000 °C for 4 h and at 1050 and 1100 °C for 2, 4 and 12 h in a muffle furnace on platinum foil.

The density of sintered samples was determined by Archimedes principle. X-ray diffraction (XRD) was used (D8 ADVANCE, parallel beam geometry,  $\text{Cu-K}\alpha$  radiation, Bruker AXS) to investigate the phase composition of calcined powders and sintered pellets (milled to powder for XRD measurement). The lattice parameter of sintered CCTO samples was calculated using Rietveld refinement (Topas software, Bruker). The microstructure of the pellet surfaces and fractures was imaged by Field Emission Scanning Electron Microscopy (FE-SEM) using Ultra 55 Zeiss equipment. Grain sizes were determined from linear intercepts of grain boundaries. Energy Dispersive X-ray (EDX) mappings and point measurements were performed with an X-Flash® 630, Bruker system. Analysis of the spectra was performed using the Quantax software package (Bruker).

For electrical measurements the sintered pellets were covered with silver paste (TC7307, Heraeus) and fired at 850 °C for 30 min. Room temperature relative permittivity was measured with an impedance analyzer (4192A, HP) in the frequency range  $f = 10 \text{ Hz} - 10^7 \text{ Hz}$ . Impedance spectra of selected samples were obtained in the same frequency range at temperatures from 120 to 500 K (Broadband Dielectric Spectrometer, Novocontrol). Separated values for the capacitance and resistance for bulk and GB regions were extracted from the impedance spectra according to the standard method [10, 19], whereby the impedance data was displayed on ZView software (Version 2.80, Scribner Associates Inc.). GB and bulk resistivity and permittivity were calculated by correcting the data with the geometrical factor  $g$  (derived from sample surface area  $A$  and thickness  $d$ ;  $g = A/d$ ).

## 3. Results and discussion

### 3.1. Phase composition

CCTO phase formation from mixed raw materials already starts during low temperature calcination at 750 °C, but residues of  $\text{CuO}$  and  $\text{TiO}_2$  precursors and secondary phase  $\text{CaTiO}_3$  were detected by XRD. At increased calcination

temperature (850 °C, 900 °C) the amount of secondary phase and raw materials reduces and finally powder prepared at 970 °C is single-phase CCTO (Fig. 1).

During sintering of compacted powders the shrinkage sets in at 770 °C and shows a maximum rate at 1005 °C (Fig. 2). Pellets sintered below 1005 °C exhibit rather poor density (Fig. 2, inset), whereas sintering at 1050 and 1100 °C results in high densities of >95 % of the theoretical value ( $\rho_{\text{theo}} = 5.04 \text{ g/cm}^3$ ). Changes in dwell time for sintering at 1050 °C had no influence on sample density, whereas prolonged sintering at 1100 °C for 4 and 12 h resulted in a small decrease of about 1 % in relative density. This may be attributed to the evaporation of an intergranular phase, which is described further below.

### 3.2. Microstructure

Figure 3 shows FE-SEM images of the surface microstructures of the sintered samples. Sintering at  $T \leq 1000$  °C leads to a homogeneous microstructure with average grain size of 1 to 2  $\mu\text{m}$  (not shown here). Sintering at 1050 °C and higher leads to the formation of a bimodal grain size distribution, i.e., small and coarse grains form. After sintering at 1050 °C the coarse grains show a broad distribution of grain size with a mean diameter of  $21 \pm 3 \mu\text{m}$ , whereas a smaller mean grain size of  $18 \pm 2 \mu\text{m}$  is observed after sintering at 1100 °C (Fig. 3). Larger grain size is expected to lead to larger capacitance and effective dielectric permittivity, and the sintering behavior seems more promising at 1050 °C for obtaining CCTO ceramics with high permittivity. For 1050 and 1100 °C sintering the number of smaller grains decreases at prolonged dwell time and more coarse grains form, but the mean grain size of the coarse grains does not change in either case.

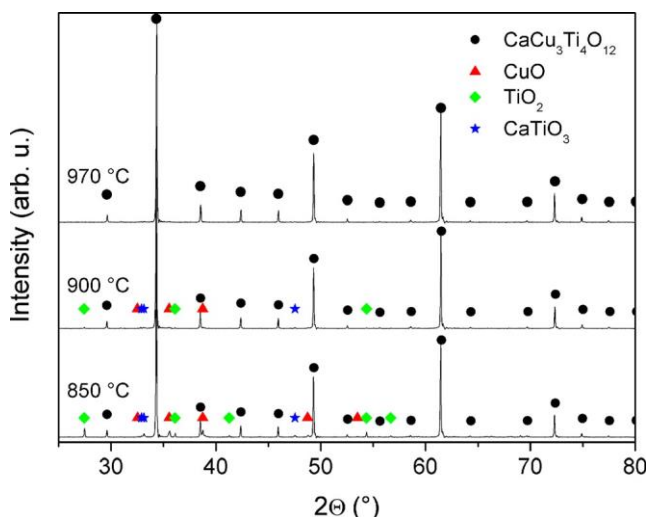


**Fig. 1** XRD pattern of powder samples after calcination for 6 h at different temperatures

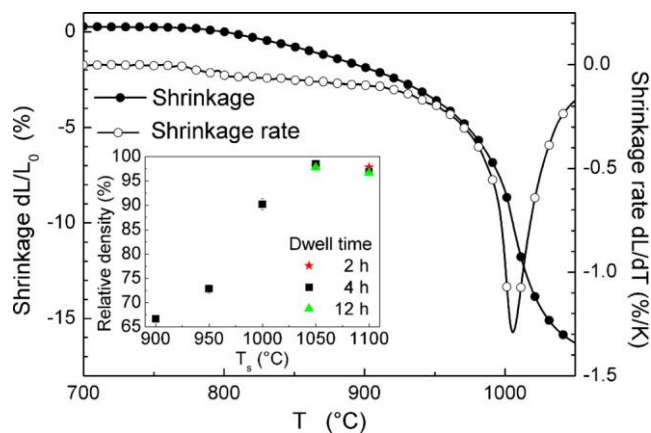


**Fig. 2** Shrinkage behavior and (inset) relative density of sintered CCTO pellets

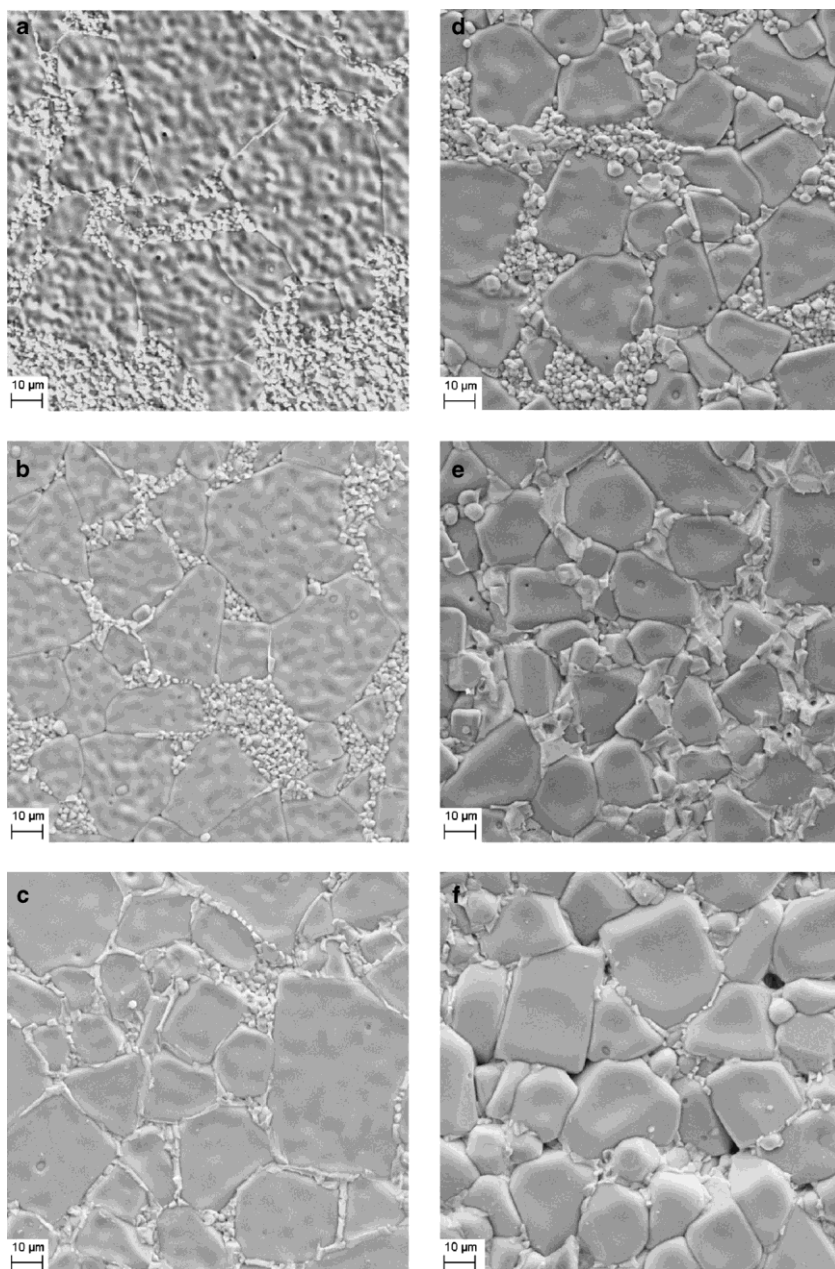
The coarse grains show a large number of intragranular pores after sintering at 1050 °C, which disappear in samples sintered at 1100 °C. After sintering at 1050 °C small  $\text{CuO}_x$ -rich grains in between islands of residual small CCTO-grains appear (Fig. 3(a) and (b)) which were detected by EDX point scans and will be discussed below (3.3). These grains may be precursors to an intergranular  $\text{CuO}_x$ -rich phase which fully forms and segregates towards the GBs at prolonged dwell time (Fig. 3(c)). After sintering at 1100 °C the coarse grains are embedded in a continuous  $\text{CuO}_x$ -rich intergranular phase looking at the sample surfaces (Fig. 3(d) and (e)). The intergranular  $\text{CuO}_x$ -rich phase was also observed in sample interior areas, but the amount of this phase is less in the interior. This is in agreement with Prakash et al. [17] who also demonstrated that a  $\text{CuO}_x$ -rich phase accumulates at the sample surfaces. The amount of intergranular phase at the sample surface reduces at 1100 °C with longer dwell time (Fig. 3(f)) which can be interpreted as a (partial) evaporation of this phase in accordance with previous reports [11, 16].

### 3.3. Composition

A more detailed EDX analysis of the surface composition of the sintered pellets demonstrates that after sintering at 1050 °C the small Cu-rich grains and the intergranular phase show low content of Ca and Ti with a Cu/Ti-atomic ratio similar to a mixture of 75 mol-% CuO – 25 mol-%  $\text{TiO}_2$  (Fig. 4). Rubia et al. [20] reported a eutectic melting point for this composition at about 1000 °C and it seems likely that the formation of the large coarse grains may be the result of a liquid-phase sintering mechanism. The Cu-rich small grains and intergranular phase observed in the FE-SEM images (Fig. 3) may be a solidified melt phase. At prolonged dwell time the Cu/Ti-atomic ratio rises (Fig. 4), indicating the progressive segregation of Cu from CCTO grains during temperature treatment.

At 1100 °C sintering with a short dwell time (2 h) the Cu/Ti-atomic ratio is higher as compared to 1050 °C and is close

**Fig. 3** FE-SEM surface images (SE images) of pellets sintered at (a) 1050 °C 2 h, (b) 1050 °C 4 h, (c) 1050 °C 12 h, (d) 1100 °C 2 h, (e) 1100 °C 4 h, (f) 1100 °C 12 h



to the composition of 96 mol-% CuO – 4 mol-% TiO<sub>2</sub> (Fig. 4) in good agreement with previous work [21]. By prolonging the dwell time at 1100 °C the Cu content of the intergranular phase increases due to CuO<sub>x</sub> segregation out of CCTO grains towards the GBs (Fig. 4), but at 12 h sintering a drop occurs, indicating the increasing evaporation.

It should be noted at this point that the determination of the intergranular phase composition is troublesome, because it cannot be completely assured that the Ti-, Ca- and Cu-signals in EDX point measurements originate exclusively from the GB phase. In fact, the surrounding CCTO grains could give a certain contribution to such signals and the exact

quantitative values measured should be considered with care. Still, the trends with sintering temperature and dwell time are believed to be reliable and in conclusion the CuO<sub>x</sub>-rich intergranular phase is likely to be formed by segregation of copper oxide during CCTO grain growth and evaporates at higher temperatures and dwell times.

This finding is further supported by the fact that EDX point measurements in the center of coarse grains show a slightly smaller Cu content than expected for a stoichiometric CCTO phase (Fig. 4), again in accordance with other reports [11, 16].

The Cu/Ti-atomic ratio within the coarse grains seems to be somewhat smaller for samples sintered at 1100 °C compared



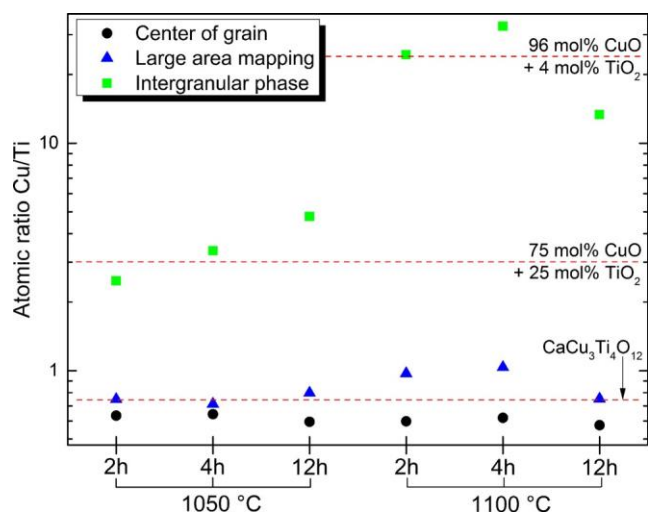


**Fig. 4** Cu/Ti-atomic ratio of intergranular phase and of CCTO coarse grains measured by EDX point scans and larger area EDX-mappings (area containing at least 20 coarse grains); the dashed lines indicate nominal Cu/Ti-atomic ratio in CuO-TiO<sub>2</sub>-mixtures and in CCTO

to those sintered at 1050 °C. This is consistent with EDX results from the intergranular phase regions. At 1100 °C the composition of the intergranular phase is more Cu-rich as compared to that after sintering at 1050 °C, hence the composition of the CCTO grains after sintering at 1100 °C needs to be somewhat more deficient in Cu. Also a small decrease of Cu/Ti-atomic ratio in the center of coarse grains is observed at prolonged dwell time (Fig. 4), imaging the dwell time dependency of the CuO<sub>x</sub> segregation process.

These observations imply that the interior areas of the coarse grains in CCTO ceramics may generally exhibit certain levels of A'-site Cu-vacancies due to such Cu loss, which may play a certain role to explain the semiconductivity in such grain interior areas as the basis of the IBLC structure. In a recent report it has been argued that A-site vacancies may be involved in the mechanism to lose lattice oxygen in titanate-based perovskites, and concomitantly affect the conductivity [22].

In addition, the overall composition of the CCTO samples sintered at 1050 °C is close to the nominal CCTO composition as demonstrated by large area EDX mappings (Fig. 4). The overall composition of samples sintered for 2 and 4 h at 1100 °C, measured through large-area mapping EDX analysis, reveals a larger Cu content than expected for the nominal CCTO composition (Fig. 4). This is likely to be due to the accumulation of the CuO<sub>x</sub>-rich intergranular phase at the sample's surface. After 12 h of sintering the overall Cu/Ti-atomic ratio drops again due to increasing evaporation of CuO<sub>x</sub> and approaches the theoretical CCTO composition. Indications of such a mechanism were reported recently based on thermogravimetry results

[11]. This may also explain the observed density decrease of pellets after prolonged sintering at 1100 °C mentioned above (Fig. 2, inset).

At this point it is worth-while to note that the intergranular phase alone cannot account for the IBLC structure in CCTO ceramics: it is well-known that the IBLC structure is fully developed after sintering CCTO ceramics at 1100 °C for longer dwell times and does not disappear, whereas the intergranular phase continuously evaporates and disappears. Therefore, the CuO<sub>x</sub>-related intergranular phase forming BETWEEN grains must be distinguished from the insulating GB phase which forms at the GB areas WITHIN the grains. It is shown here though that the intergranular phase clearly influences the GB phase and its dielectric properties due to the direct contact of the two phases and/or the liquid phase sintering behavior facilitated.

### 3.4. Lattice parameters

X-ray diffraction of sintered samples reveals single CCTO phase. No diffraction peaks of copper oxide are detected indicating that the amount of CuO<sub>x</sub>-rich intergranular phase is small and below the detection limit of XRD. The lattice parameters of sintered CCTO samples are larger as compared to calcined powder ( $a_0 = 7.3920(1)$  Å) and increase nearly linearly with higher sintering temperature (Fig. 5) in agreement with previous work [11]. It was demonstrated more recently though that the lattice parameters of Cu-deficient CCTO samples increase compared to nominally stoichiometric material [19]. If CuO<sub>x</sub>-segregation is assumed to be accompanied by a partial evaporation of the formed CuO<sub>x</sub>-rich intergranular phase at increasing temperature this would consequently result in Cu deficiency of the remaining CCTO grain interior, which was also deduced from EDX point scans

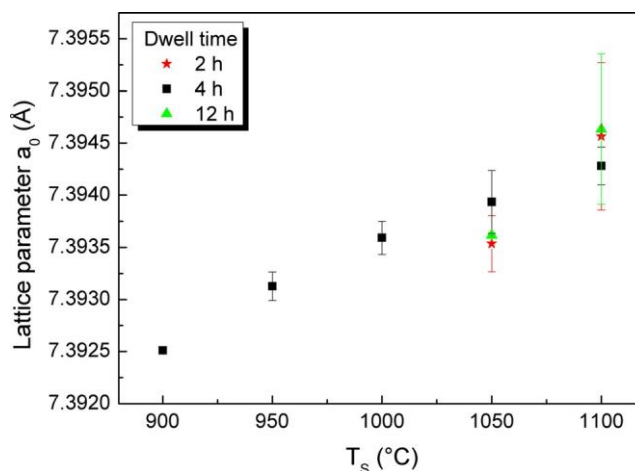


**Fig. 5** Variation of lattice parameter  $a_0$  as a function of sintering temperature and dwell time

(Fig. 4). This can explain the increase in lattice parameter with sintering temperature. The dwell time shows no significant influence on lattice parameter  $a_0$ . Therefore the segregation process of  $\text{CuO}_x$  from the bulk towards the GBs seems to be less influenced by sintering time than by sintering temperature.

### 3.5. Electrical properties

The effective dielectric permittivity  $\epsilon'$  of the sintered samples is shown in Fig. 6 vs.  $f$ . Samples sintered below 1000 °C show modest room temperature  $\epsilon'$  only, which then increases with increasing sintering temperature (Fig. 6(a)). Samples sintered at 1050 and 1100 °C exhibit the typical permittivity behavior of CCTO ceramics already reported in many studies. High effective permittivity was measured up to a frequency of about  $10^6$  Hz followed by a typical relaxation of CCTO that is accompanied by a loss peak of the imaginary part of permittivity (Fig. 6(b)) and a drop of effective permittivity down to  $\epsilon' \approx 100$  [2, 3, 7]. The largest permittivity values were achieved for sintering at 1050 °C, which highlights the important effect of the intergranular phase on the permittivity. Fig. 6(a) shows that 1050 °C sintered CCTO ceramics exhibit the highest dielectric permittivity and the liquid phase sintering behavior of the intergranular phase mentioned above appears to be optimal at 1050 °C for obtaining ceramics with slightly increased grain size and increased dielectric permittivity. Longer dwell time during sintering at the preferred 1050 °C leads to an increase of effective permittivity, but shifts sample-electrode-interaction effects to larger  $f$ . On the other hand, samples that were sintered at 1100 °C show a small decrease of effective permittivity at prolonged dwell time (Fig. 6(a), inset). This is not in agreement with several previous reports [16–18], but may be associated with the decrease of density observed here, which was argued above to possibly occur due to the (partial) evaporation of the intergranular phase.

An additional permittivity contribution appears at low  $f$  (Fig. 6(a)), which was attributed to a sample-electrode-interaction. The electrode effect was quite small after sintering at 1100 °C and large after sintering at 1050 °C. Other electrode materials such as Cu (sputtered on the sample surfaces) and InGa paste (heat treated after application) were tested for potentially improved sample-electrode-interaction, but gave no better results (Fig. 6(c)).

The temperature trends of relative dielectric permittivity  $\epsilon'$  and electrical resistivity  $\rho$  of bulk grain and GB regions of CCTO samples were evaluated using temperature dependent impedance spectroscopy. As an example, the impedance plot ( $-Z''$  vs.  $Z'$ ) of a sample sintered at 1000 °C is shown in Fig. 7.

The semicircle representing the bulk interior grain regions (semicircle diameter=resistivity) is only measurable at the lowest temperatures (120 K, Fig. 7, right inset) due to low bulk permittivity  $\epsilon_{\text{bulk}}$  and low semiconducting bulk resistivity  $\rho_{\text{bulk}}$  and therefore, only a few data points of  $\epsilon_{\text{bulk}}$  could be extracted from the measured spectra.  $\epsilon_{\text{bulk}}$  was determined

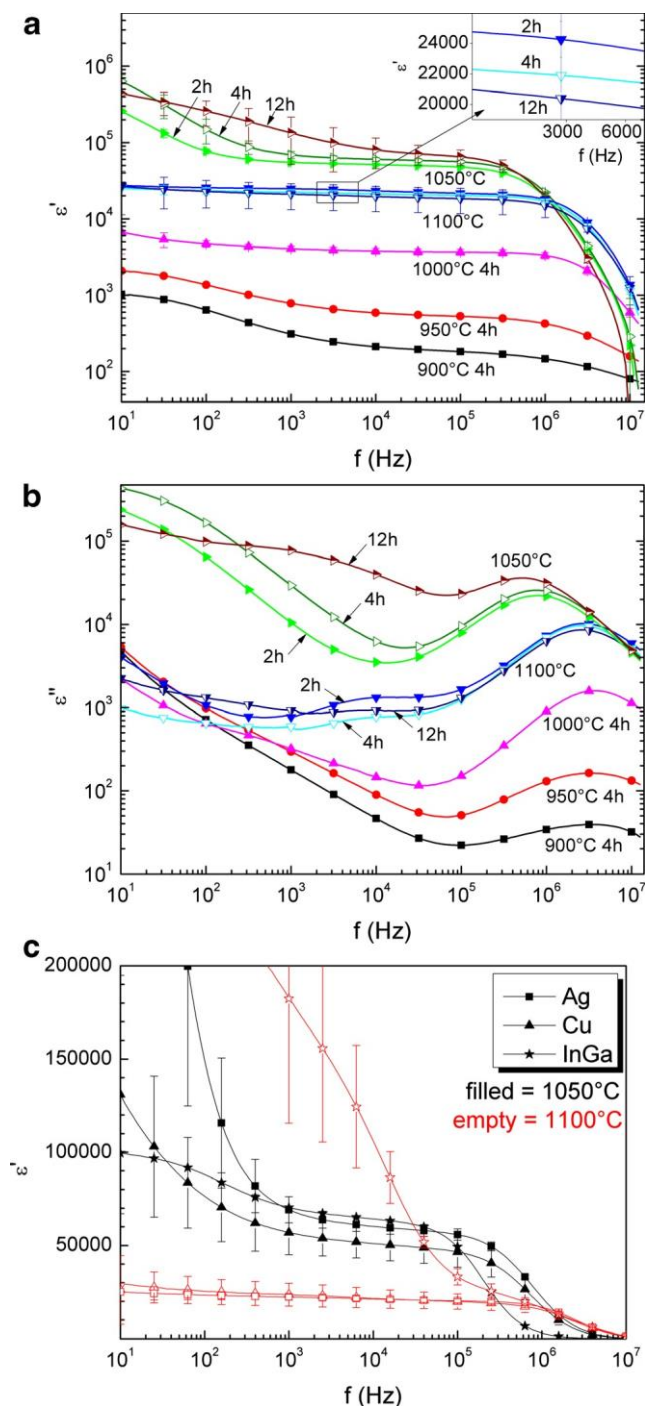


**Fig. 6** (a) Real and (b) imaginary part of room temperature permittivity of CCTO pellets sintered at 900, 950, 1000, 1050 and 1100 °C and (c) effect of different electrode materials on effective permittivity of CCTO samples sintered at 1050 and 1100 °C for 4 h

from the frequency at the bulk semicircle maximum  $f_{\max}=1/(2\pi\rho_{\text{bulk}}\cdot\epsilon_{\text{bulk}})$ . The equivalent relationship is valid for the GB contribution as well. Measurements at room temperature and above (440 K) display a semicircle that is assigned to the GB phase, superimposed with a second semicircle due to the sample-electrode-interaction. Still, the bulk resistivity  $\rho_{\text{bulk}}$  can be determined quite reliably from the non-zero intercept of the high- $f$  data with the real  $Z'$  axis (Fig. 7, left inset). The CCTO grains show low  $\epsilon_{\text{bulk}}=80\text{--}110$ . However, if one takes into account a certain experimental error (10 %), a possible trend can be recognized of slightly increasing  $\epsilon_{\text{bulk}}$  with dwell time for sintering at 1050 and at 1100 °C (not shown here).

According to the IBL model, GBs are expected to be electrically insulating and the bulk of grains to be semiconducting. Analysis of IS data revealed that the GB and bulk resistivity,  $\rho_{\text{gb}}$  and  $\rho_{\text{bulk}}$ , differ by some orders of magnitude whereas the activation energies  $E_A$  differ by a factor of  $\approx 7$  (Fig. 8 and Table 1).  $\rho_{\text{gb}}$  is large for sintering at 1000 °C, but reduces at higher sintering temperatures and is smallest for 1050 °C (Fig. 8). This minimum at 1050 °C where the intergranular phase has a high concentration again pronounces the role of this phase on the GB dielectric properties. This minimum encountered is somewhat different though to previous work [10, 11] where a consistent trend of decreasing  $\rho_{\text{gb}}$  with increasing sintering temperature has been reported, but for longer dwell times. This implies that the shorter dwell times employed here reveal a more complex formation behavior of the IBL structure where the intergranular phase may in fact play an integral role for the sinter-behavior, because it is expected to promote liquid phase sintering. As mentioned above, the Cu/Ti-atomic ratio of the intergranular phase may be important, but also the effect of other impurities should be considered. The starting powders used here in this study have an inferior purity as compared to the powders used in

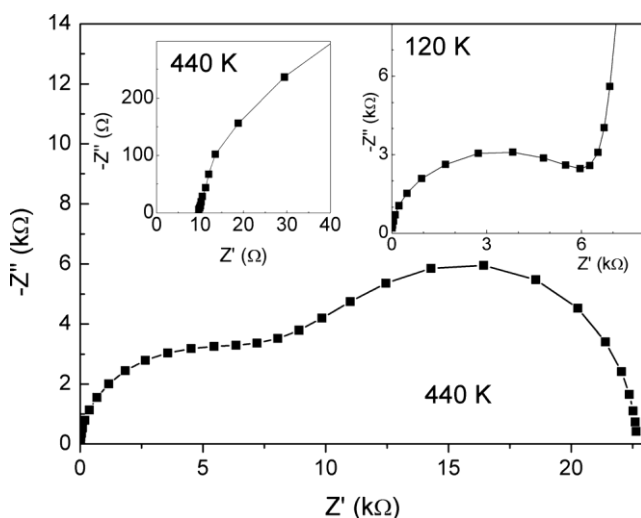


**Fig. 7** Complex impedance plot  $-Z''$  vs.  $Z'$  of a pellet sintered for 4 h at 1000 °C (insets: magnified regions near the origin at  $T=440$  K (left) and  $T=120$  K (right))

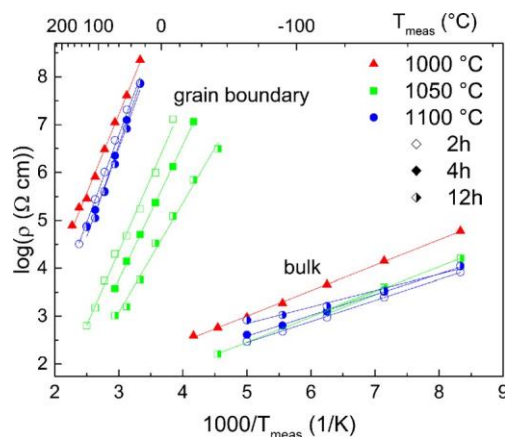


**Fig. 8** GB and bulk resistivity of CCTO samples sintered at different temperatures and dwell times

references [10, 11], which may serve as an alternative explanation for the different trends of dielectric behavior vs. sintering temperature observed.

For sintering at 1050 °C  $\rho_{\text{gb}}$  and  $E_{A,\text{gb}}$  decrease with prolonged dwell time (Fig. 8 and Table 1). For sintering at 1100 °C the  $\rho_{\text{gb}}$  decreases with longer dwell time as well, yet the change is smaller, whereas the trend of  $E_{A,\text{gb}}$  is not fully clear but the nominal  $E_{A,\text{gb}}$  values are all larger than for the 1050 °C samples.

$\rho_{\text{bulk}}$  shows high values after sintering at 1000 °C and decreases at higher sintering temperature (Fig. 8). However,  $\rho_{\text{bulk}}$  is quite similar for sintering at 1050 and 1100 °C and the intergranular phase only seems to affect the GB behavior, which is in fact quite expected. The activation energy of the bulk resistivity is around 0.1 eV for samples sintered at 1000 °C and 1050 °C and decreases to  $E_{A,\text{bulk}}=0.08\text{--}0.09$  eV for samples sintered at 1100 °C (Table 1) in agreement with values reported in the literature [7]. It is noted that the effect of dwell time is more distinct on the electrical properties of GB for sintering at 1050 °C and 1100 °C, which again may indicate that the intergranular phase is at play here. Dwell time dependent changes of  $\rho_{\text{bulk}}$  at these sintering temperatures are small.

Major compositional changes in the bulk seem to happen at the early stages of sintering whereby the process of segregation of a  $\text{CuO}_x$ -related phase towards the intergranular regions largely influences the GB dielectric properties. This effect is

**Table 1** Change of bulk and grain boundary activation energy at varied dwell times

	$E_{A,\text{bulk}}$ (eV)			$E_{A,\text{gb}}$ (eV)		
	1000 °C	1050 °C	1100 °C	1000 °C	1050 °C	1100 °C
2 h	–	0.104	0.087	–	0.604	0.741
4 h	0.105	0.104	0.086	0.650	0.558	0.770
12 h	–	0.104	0.080	–	0.441	0.730

clearly pronounced at 1050 °C, whereas sintering at 1100 °C may lead to much quicker evaporation of the intergranular phase and its effect on the GB dielectric properties is less pronounced.

#### 4. Conclusions

CCTO ceramics sintered at  $T > 1000$  °C exhibit grain growth and the formation of an inhomogeneous microstructure. For sintering at 1050 °C small CCTO and Cu-rich grains vanish at prolonged dwell time and a continuous Cu-rich intergranular phase develops between large grains enabling liquid phase sintering. For sintering at 1100 °C with short dwell time already a continuous  $\text{CuO}_x$ -rich intergranular phase has formed and is accumulated at the sample's surfaces. The overall sample composition is consistent to the nominal CCTO composition, but EDX of coarse grains revealed small Cu-deficiency indicating a segregation process of copper oxide and the formation of a  $\text{CuO}_x$ -rich intergranular phase during sintering.

At prolonged dwell time the effective permittivity increases at 1050 °C, but shows small reduction after sintering at 1100 °C. The GB resistivity shows the same trend for both sintering temperatures: it decreases with longer dwell time. Compositional changes in the bulk are little, therefore only small changes of bulk properties are observed at prolonged sintering time. On the other hand, compositional changes in the GBs such as  $\text{CuO}_x$  segregation are reflected in the observed dwell time dependent electrical properties.

The formation of the IBLC structure may be understood as follows: at low sintering temperature CCTO is fully insulating [23]. With increasing temperature the semiconducting grain interior phase forms due to segregation of Cu-rich material towards the grain boundaries, i.e., semiconducting grain interior areas are Cu-deficient and insulating GB areas are Cu-rich. The thickness of the Cu-rich GB areas reduce with increasing temperature due to increased  $\text{CuO}_x$  segregation and at 1050 °C a  $\text{CuO}_x$ -rich intergranular phase starts forming. As demonstrated here, the Cu/Ti-atomic ratio of this intergranular phase changes with sintering temperature and dwell time, which influences the GB dielectric properties. Therefore, the Cu concentration in the GBs alone cannot account for the GB dielectric properties, but the composition of and the liquid

phase sintering enabled by the intergranular phase need to be considered for engineering well-controlled IBLC structures with high-permittivity GB areas in CCTO ceramics.

**Acknowledgments** This work was supported by the State of Thuringia, Germany, through a grant in the ProExzellenz network (Kerfunmat, PE 214). R.S. wishes to acknowledge a Ramón y Cajal fellowship from the MICINN/MINECO (Spain).

#### References

1. M.A. Subramanian, A.W. Sleight, *Solid State Sci.* **4**, 347 (2002)
2. T.B. Adams, D.C. Sinclair, A.R. West, *Adv. Mater.* **14**, 1321 (2002)
3. A.R. West, T.B. Adams, F.D. Morrison, D.C. Sinclair, *J. Eur. Ceram. Soc.* **24**, 1439 (2004)
4. M.A. Subramanian, D. Li, N. Duan, B.A. Reisner, A.W. Sleight, *J. Solid State Chem.* **151**, 323 (2000)
5. J. Sebal, S. Krohns, P. Lunkenheimer, S.G. Ebbinghaus, S. Riegg, A. Reller, A. Loidl, *Solid State Commun.* **150**, 857 (2010)
6. A.J. Moulson, J.M. Herbert, *Electroceramics*, 2nd edn. (Wiley, Chichester, 2003), p. 327
7. D.C. Sinclair, T.B. Adams, F.D. Morrison, A.R. West, *Appl. Phys. Lett.* **80**, 2153 (2002)
8. T.B. Adams, D.C. Sinclair, A.R. West, *Phys. Rev. B* **73**, 094124 (2006)
9. J.T.S. Irvine, D.C. Sinclair, A.R. West, *Adv. Mater.* **2**, 132 (1990)
10. R. Schmidt, in *Ceramic Materials Research Trends*, ed. by P.B. Lin (Novascience Publishers, Hauppauge, 2007), p. 321
11. R. Schmidt, M.C. Stennett, N.C. Hyatt, J. Pokorny, J. Prado-Gonjal, M. Li, D.C. Sinclair, *J. Eur. Ceram. Soc.* **32**, 3313 (2012)
12. J. Li, M.A. Subramanian, H.D. Rosenfeld, C.Y. Jones, B.H. Toby, A.W. Sleight, *Chem. Mater.* **16**, 5223 (2004)
13. J. Li, A.W. Sleight, M.A. Subramanian, *Solid State Commun.* **135**, 260 (2005)
14. D. Capsoni, M. Bini, V. Massarotti, G. Chiodelli, M.C. Mozzatic, C.B. Azzoni, *J. Solid State Chem.* **177**, 4494 (2004)
15. L. Ni, X.M. Chen, X.Q. Liu, R.Z. Hou, *Solid State Commun.* **139**, 45 (2006)
16. J.J. Romero, P. Leret, F. Rubio-Marcos, A. Quesada, J.F. Fernández, *J. Eur. Ceram. Soc.* **30**, 737 (2010)
17. B.S. Prakash, K.B.R. Varma, *J. Phys. Chem. Solids* **68**, 490 (2007)
18. C.-M. Wang, K.-S. Kao, S.-Y. Lin, Y.-C. Chen, S.-C. Wenig, *J. Phys. Chem. Solids* **69**, 608 (2008)
19. R. Schmidt, S. Pandey, P. Fiorenza, D.C. Sinclair, *RSC Adv.* **3**, 14580 (2013)
20. M.A. de la Rubia, J.J. Reinoso, P. Leret, J.J. Romero, J. de Frutos, J.F. Fernández, *J. Eur. Ceram. Soc.* **32**, 71 (2012)
21. P. Leret, J.F. Fernandez, J. de Frutos, D. Fernández-Hevia, *J. Eur. Ceram. Soc.* **27**, 3901 (2007)
22. I. Akin, M. Li, Z. Lu, D.C. Sinclair, *RSC Adv.* **4**, 32594 (2014)
23. S.I.R. Costa, M. Li, J.R. Frade, D.C. Sinclair, *RSC Adv.* **3**, 7030 (2013)